Turbulence-Free Double-slit Interferometer

Thomas A. Smith and Yanhua Shih

Department of Physics, University of Maryland, Baltimore County, Baltimore, Maryland 21250, USA

Optical turbulence can be detrimental for optical observations. For instance, atmospheric turbulence may reduce the visibility or completely blur out the interference produced by an interferometer in open air. However, a simple two-photon interference theory based on Einstein's granularity picture of light makes a turbulence-free interferometer possible; i.e., any refraction index, length, or phase variations along the optical paths of the interferometer do not have any effect on its interference. Applying this mechanism, the reported experiment demonstrates a two-photon double-slit interference that is insensitive to atmospheric turbulence. The turbulence-free mechanism and especially the turbulence-free interferometer would be helpful in optical observations that require high sensitivity and stability such as for gravitational-wave detection.

Since Young invented his double-slit (double-pinhole) interferometer in 1807 [1,2], interference phenomena have played an important role in our fundamental understanding of nature and have had practical applications in almost all fields of science [3–7]. It is well known that optical turbulence is harmful in optical observations. Random variations in the composition or density of the medium lead to changes in the index of refraction, known as optical turbulence, and thus vary the relative phases between different optical paths of an interferometer. These variations may "blur" the interference pattern partially or completely, thus reducing the sensitivity and effectiveness of an interferometer [8,9]. This turbulence is particularly detrimental for extremely sensitive interferometers, interferometric spectrometers, and other interferometer based sensors, for instance, those used in gravitational-wave detectors like the Laser Interferometer Gravitational-Wave Observatory (LIGO) [10,11], which must be placed in a high-cost vacuum. Here, we report an experimental study of a turbulence-free two-photon double-slit interferometer.

As depicted in the schematic setup of the experiment, Fig. 1, the demonstrated interferometer is a classic Young's double-slit interferometer except that it has two pointlike, scannable photon counting detectors D_1 and D_2, rather than one. Together they measure the photon number fluctuation correlation $\langle \Delta n(x_1) \Delta n(x_2) \rangle$ or the intensity fluctuation correlation $\langle \Delta I(x_1) \Delta I(x_2) \rangle$ [12]. In fact, this interferometer is able to produce three outputs corresponding to two types of measurement: (1) $\langle n(x_1) \rangle \propto \langle I(x_1) \rangle$ and $\langle n(x_2) \rangle \propto \langle I(x_2) \rangle$, corresponding to the measurement of mean intensities at D_1 and D_2, respectively; (2) $\langle \Delta n(x_1) \Delta n(x_2) \rangle \propto \langle \Delta I(x_1) \Delta I(x_2) \rangle$, corresponding to the measurement of the intensity fluctuation correlation at D_1 and D_2, jointly. In this experiment, we managed to have the spatial coherence length l_c of the field much smaller than the separation d

between the upper slit (slit A) and the lower slit (slit B), $l_c \ll d$, where $l_c = \lambda / \Delta \theta_s$ with λ the wavelength of the monochromatic thermal radiation, and $\Delta \theta_s$ the angular diameter of the light source [2,12]. Consequently, no first-order interferences are observable from $\langle I(x_1) \rangle$ and $\langle I(x_2) \rangle$. However, an interference pattern with 100% visibility is observed from the measurement of $\langle \Delta n(x_1) \Delta n(x_2) \rangle \propto \langle \Delta I(x_1) \Delta I(x_2) \rangle$ and the interference is insensitive to any refractive index variations and atmospheric vibration induced phase variations in the optical path of the interferometer; namely, it is turbulence free when scanning D_1 and D_2 in the neighborhood of $x_1 \approx x_2$.

How could interference appear from the measurement of the intensity fluctuation correlation? And why is it turbulence free? Recall, in 1905, Einstein introduced a granularity to radiation, abandoning the continuum interpretation of Maxwell. This led to a microscopic picture of radiation and a statistical view of light [13]. In Einstein's picture, a natural light source, such as the sun or a distant star, consists of many pointlike subsources ("atomic transitions" in modern language), each of which emit their own subfields (originally labeled in German by *strahlenbündel*, translated to "bundle of ray" in English, and now labeled as "photon" in modern language) in a random manner: the mth subfield (photon) that is emitted from the mth pointlike subsource (atomic transition) may propagate in all possible directions with any random phase. This kind of light has the popular name "thermal light" due to its chaotic nature. It has been proven that for a defined quantum state, such as the thermal state, an effective wave function of a photon can be calculated from the quantum theory of optical coherence [14]. The effective wave function of a photon in the thermal state is mathematically the same function as Einstein's subfield [12,15]. In Einstein's picture, the radiation measured at coordinate $(\mathbf{r}, t)$ is the result of a superposition among a large number of subfields,
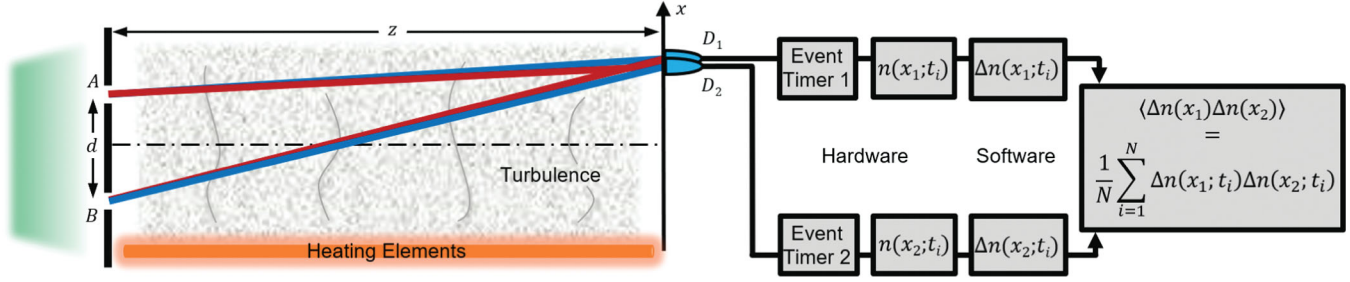
FIG. 1. A turbulence-free double-slit interferometer. This interferometer has two types of output: (1) $\langle n(x_1) \rangle \propto \langle I(x_1) \rangle$ and $\langle n(x_2) \rangle \propto \langle I(x_2) \rangle$, and (2) $\langle \Delta n(x_1)\Delta n(x_2) \rangle \propto \langle \Delta I(x_1)\Delta I(x_2) \rangle$. Because of the experimental condition of $d \gg l_c$, no interferences are observable from $\langle I(x_1) \rangle$ and $\langle I(x_2) \rangle$. However, a turbulence-free interference with 100% visibility is observed from the measurement of $\langle \Delta n(x_1)\Delta n(x_2) \rangle$. The observed interference is a two-photon phenomenon: a random pair of photons interfering with the pair itself. In the figure, the superposed two different yet indistinguishable two-photon amplitudes are indicated by red and blue colors. When the detectors are scanning in the neighborhood of $x_1 \approx x_2$, the red amplitude and the blue amplitude "overlap," which means the pair experiences the same phase variations, and thus the interference is turbulence free. The turbulence starts reducing the visibility after ~ten periods from $x_1 = x_2$.

$$E(\mathbf{r}, t) = \sum_m E_m(\mathbf{r}_m, t_m) g_m(\mathbf{r}_m, t_m; \mathbf{r}, t), \quad (1)$$

where $E_m(\mathbf{r}_m, t_m)$ labels the subfield emitted from the mth subsource at coordinate $(\mathbf{r}_m, t_m)$, and $g_m(\mathbf{r}_m, t_m; \mathbf{r}, t)$ represents the field propagator or Green's function that propagates the mth subfield from coordinate $(\mathbf{r}_m, t_m)$ to coordinate $(\mathbf{r}, t)$ [12]. For free propagation, such as the propagation of a subfield from the subsource to the double slit (or from the double slit to a detector), the Green's function is of the form

$$g_m(\mathbf{r}_m, t_m; \mathbf{r}, t) = e^{i(\mathbf{k}\cdot(\mathbf{r}-\mathbf{r}_m)-\omega(t-t_m))}. \quad (2)$$

If there exists more than one different yet indistinguishable path or alternative for the mth subfield to propagate from $(\mathbf{r}_m, t_m)$ to $(\mathbf{r}, t)$, $g_m(\mathbf{r}_m, t_m; \mathbf{r}, t)$ must be written as a superposition

$$g_m(\mathbf{r}_m, t_m; \mathbf{r}, t) = \frac{1}{\sqrt{N}} \sum_{s=1}^N g_{ms}(\mathbf{r}_m, t_m; \mathbf{r}, t). \quad (3)$$

Shortening the notation, we will replace $E_m(\mathbf{r}_m, t_m)$ with E_m and $g_m(\mathbf{r}_m, t_m; \mathbf{r}, t)$ with $g_m(\mathbf{r}, t)$. The measured intensity corresponds to its statistical expectation value

$$\langle I(\mathbf{r}, t) \rangle = \left\langle \sum_m E_m^*(\mathbf{r}, t) \sum_n E_n(\mathbf{r}, t) \right\rangle$$

$$= \left\langle \sum_m |E_m(\mathbf{r}, t)|^2 \right\rangle + \left\langle \sum_{m \neq n} E_m^*(\mathbf{r}, t) E_n(\mathbf{r}, t) \right\rangle$$

$$= \sum_m |E_m(\mathbf{r}, t)|^2 + 0. \quad (4)$$

We may conclude that the mean intensity is the result of the mth subfield interfering with the mth subfield itself. The interferences between different subfields, corresponding to

the $m \neq n$ term, vanish when taking into account all possible random phases of the subfields. If a measurement deals with a limited number of subfields and their phases do not take all possible random values, $\sum_{m \neq n} E_m^*(\mathbf{r}, t) E_n(\mathbf{r}, t)$ may not vanish. In this case, the interferences between different subfields contribute a "noise" $\Delta I(\mathbf{r}, t)$ to the measurement of $\langle I(\mathbf{r}, t) \rangle$,

$$\Delta I(\mathbf{r}, t) = \sum_{m \neq n} E_m^*(\mathbf{r}, t) E_n(\mathbf{r}, t). \quad (5)$$

Assuming we have a measurement device that is able to measure the intensity fluctuation correlation by means of a correlation circuit and two independent and spatially separated photodetectors, either in analog mode, which measures $\langle \Delta I(\mathbf{r}_1, t_1) \Delta I(\mathbf{r}_2, t_2) \rangle$, or in photon counting mode, which measures $\langle \Delta n(\mathbf{r}_1, t_1) \Delta n(\mathbf{r}_2, t_2) \rangle$,

$$\langle \Delta I(\mathbf{r}_1, t_1) \Delta I(\mathbf{r}_2, t_2) \rangle$$

$$= \left\langle \sum_{m \neq n} E_m^*(\mathbf{r}_1, t_1) E_n(\mathbf{r}_1, t_1) \sum_{p \neq q} E_p^*(\mathbf{r}_2, t_2) E_q(\mathbf{r}_2, t_2) \right\rangle$$

$$= \sum_{m \neq n} E_m^*(\mathbf{r}_1, t_1) E_n(\mathbf{r}_1, t_1) E_n^*(\mathbf{r}_2, t_2) E_m(\mathbf{r}_2, t_2), \quad (6)$$

due to the random relative phases between the subfields, the only surviving terms in the above summation are the $m = q$ and $n = p$ terms. Mathematically, the result of Eq. (6) is the cross term of the following superposition

$$\sum_{m \neq n} |E_m(\mathbf{r}_1, t_1) E_n(\mathbf{r}_2, t_2) + E_n(\mathbf{r}_1, t_1) E_m(\mathbf{r}_2, t_2)|^2, \quad (7)$$

corresponding to the superposition of two different yet indistinguishable alternatives of joint photodetection: (1) the mth subfield is measured at $(\mathbf{r}_1, t_1)$ while the nth subfield is measured at $(\mathbf{r}_2, t_2)$; (2) the nth subfield is

measured at $(\mathbf{r}_1, t_1)$ while the mth subfield is measured at $(\mathbf{r}_2, t_2)$. Physically, the above superposition defines a two-photon interference: a random pair of subfields (photons) interferes with the pair itself.

To see why the measurement of $\langle \Delta n(\mathbf{r}_1, t_1) \Delta n(\mathbf{r}_2, t_2) \rangle$ is turbulence free, it might be helpful to recall why the classic Young's double-slit interferometer is turbulence sensitive. In Dirac's language [16], the interference observed from a classic Young's double-slit interferometer is a single photon phenomenon: a photon interfering with the photon itself. The interference patterns measured in $\langle I(x_1) \rangle$ and $\langle I(x_2) \rangle$ are calculated as follows:

$$
\begin{aligned}
\langle I(x_j) \rangle &= \sum_m |E_m g_m(x_j, t_j)]|^2 \\
&= \sum_m |E_m \frac{1}{\sqrt{2}} [g_{mA}(x_j, t_j) + g_{mB}(x_j, t_j)]|^2 \\
&= \sum_m |E_m|^2 | \frac{1}{\sqrt{2}} [g_m(\mathbf{r}_A, t_A) g_A(x_j, t_j) \\
&\quad + g_m(\mathbf{r}_B, t_B) g_B(x_j, t_j)]|^2,
\end{aligned}
\tag{8}
$$

where $g_m(x_j, t_j) = [g_{mA}(x_j, t_j) + g_{mB}(x_j, t_j)]/\sqrt{2}$, for $j = 1, 2$, is the Green's function that propagates the mth subfield from the source to D_j at (x_j, t_j), indicated by a red path and a blue path in Fig. 1, where A labels the upper path (passing slit A), and B labels the lower path (passing slit B). We have denoted $g_{mA}(x_j, t_j) = g_m(\mathbf{r}_A, t_A) g_A(x_j, t_j)$ and $g_{mB}(x_j, t_j) = g_m(\mathbf{r}_B, t_B) g_B(x_j, t_j)$ with $g_m(\mathbf{r}_A, t_A)$ and $g_m(\mathbf{r}_B, t_B)$ being the Green's functions propagating the mth subfield from the mth subsource to slit A and slit B, respectively, and $g_A(x_j, t_j)$ and $g_B(x_j, t_j)$ being the Green's functions propagating the field from slit A and slit B to D_j at (x_j, t_j), respectively. For a continuous source with angular size $\Delta\theta_s$, the summation can be approximated as an integral from $-\Delta\theta_s/2$ to $\Delta\theta_s/2$. Because of $g_m(\mathbf{r}_A, t_A)$ and $g_m(\mathbf{r}_B, t_B)$ both being present in the cross terms of Eq. (8), this integral results in a sinc function and the remaining Green's functions, $g_A(x_j, t_j)$ and $g_B(x_j, t_j)$, contribute to a cosine function [12], giving us

$$
\langle I(x_j) \rangle = I_0 \left[1 + \mathrm{sinc} \frac{\pi d \Delta\theta_s}{\lambda} \cos \frac{2\pi d}{\lambda z} x_j \right],
\tag{9}
$$

where z is the distance between the slits and the detector and the sinc function is defined as $\mathrm{sinc}(x) = \sin(x)/x$. It is easy to see that (1) when $d > \lambda/\Delta\theta_s$, i.e., $d > l_c$, there would be no observable interference and (2) one can never make the red path and the blue path of the mth subfield overlap unless one makes $d \to 0$.

In contrast, Eq. (7) indicates that the interference observed from $\langle \Delta n(\mathbf{r}_1, t_1) \Delta n(\mathbf{r}_2, t_2) \rangle$ is a two-photon interference phenomenon. However, this two-photon interference is different from the historical two-photon

double-slit interference that involves the superposition of two-photon amplitudes of an entangled photon pair [17–22]. The two-photon interference indicated in Eq. (7), introduced by Scarcelli et al. [23], involves the superposition of two-photon amplitudes of a random pair of photons in the thermal state. Substituting the Green's functions into Eq. (7), the superposition can be written as

$$
\begin{aligned}
\sum_{m \neq n} &|E_m g_m(x_A, t_A) g_A(x_1, t_1) E_n g_n(x_B, t_B) g_B(x_2, t_2) \\
&+ E_m g_m(x_A, t_A) g_A(x_2, t_2) E_n g_n(x_B, t_B) g_B(x_1, t_1)|^2
\end{aligned}
$$

and its cross term results in a sinusoidal function of $(x_1 - x_2)$:

$$
\begin{aligned}
&\langle \Delta I_{AB}(x_1, t_1) \Delta I_{AB}(x_2, t_2) \rangle \\
&= \sum_{m \neq n} E_m^* g_m^*(x_A, t_A) g_A^*(x_1, t_1) E_n g_n(x_B, t_B) g_B(x_1, t_1) \\
&\quad \times E_n^* g_n^*(x_B, t_B) g_B^*(x_2, t_2) E_m g_m(x_A, t_A) g_A(x_2, t_2) \\
&= \sum_{m \neq n} |E_m|^2 |E_n|^2 g_A^*(x_1, t_1) g_B(x_1, t_1) g_A(x_2, t_2) g_B^*(x_2, t_2) \\
&= I_0^2 \cos \frac{2\pi d}{\lambda z} (x_1 - x_2).
\end{aligned}
\tag{10}
$$

Two differences are apparent when comparing Eqs. (8) and (10): (1) unlike the interference in the measurement of $\langle I(x_1) \rangle$ and $\langle I(x_2) \rangle$, in Eq. (10), $|g_m(x_A, t_A)|^2 = 1$ and $|g_n(x_B, t_B)|^2 = 1$, removing the sinc function but leaving the cosine function, which means the visibility of the interference modulation does not depend on the angular size of the light source, $\Delta\theta_s$, or on the spatial coherence length l_c, and (2) it is possible to overlap the two-photon amplitudes when scanning in the neighborhood of $x_1 \approx x_2$ (as demonstrated in Fig. 1) and still keep the interference observable when $d \gg l_c$.

In addition to the above alternatives for the mth and the nth subfields to produce a joint photodetection event of D_1 and D_2, the mth and the nth subfields can also produce a joint photodetection event when both pass through slit A or both pass through slit B. These two alternatives contribute constants to $\langle \Delta I(x_1) \Delta I(x_2) \rangle$. Adding the contributions from all alternatives, we have an observable turbulence-free interference in the neighborhood of $x_1 \approx x_2$ with 100% visibility [23],

$$
\begin{aligned}
&\langle \Delta I(x_1) \Delta I(x_2) \rangle \\
&= \langle \Delta I_{AB}(x_1, t_1) \Delta I_{AB}(x_2, t_2) \rangle + \langle \Delta I_{BA}(x_1, t_1) \Delta I_{BA}(x_2, t_2) \rangle \\
&\quad + \langle \Delta I_{AA}(x_1, t_1) \Delta I_{AA}(x_2, t_2) \rangle + \langle \Delta I_{BB}(x_1, t_1) \Delta I_{BB}(x_2, t_2) \rangle \\
&= I_0^2 \left[1 + \cos \frac{2\pi d}{\lambda z} (x_1 - x_2) \right].
\end{aligned}
\tag{11}
$$

To simplify the photon number fluctuation correlation circuit, we have employed a standard monochromatic

pseudothermal light source [24] consisting of a rotating ground glass and a single-frequency laser beam of wavelength $\lambda = 532$ nm. Millions of tiny diffusers within the rotating ground glass scatter the laser beam into many independent wave packets, or subfields, at the single-photon level with random relative phases, artificially simulating a natural thermal light source such as the sun. Directly following the ground glass is an adjustable pinhole used to control the transverse size of the light source, allowing us to alter the spatial coherence length of the thermal field. A double slit with $d = 2.5$ mm and linelike slits is then placed 1.6 m after the pinhole. Using this, we simulated a thermal light source with an angular diameter of $\Delta\theta_s \approx 0.00156$ and thus obtained a spatial coherence length of $l_c = \lambda/\Delta\theta_s \approx 0.34$ mm, satisfying $d \gg l_c$. In this case, no interference is observable from $\langle n(x_1) \rangle \propto \langle I(x_1) \rangle$ and $\langle n(x_2) \rangle \propto \langle I(x_2) \rangle$.

After passing through the double slit, wave packets (subfields) propagate to the observation plane and meet the pointlike tips of two single-mode optical fibers, which are able to be scanned along the x axis by two step motors. These fibers direct the light to photon counting detectors D_1 and D_2. The pointlike tips of the optical fibers allow for the collection of light at $x_1 \approx x_2$ and, to allow further overlap of x_1 and x_2, the two optical fiber tips were placed on either side of a beam splitter (not pictured in Fig. 1).

A photon number fluctuation correlation circuit [25,26] is used to measure the photon number fluctuation correlation for each chosen value of $(x_1 - x_2)$. The photon number fluctuation correlation circuit has two synchronized event timers to record the registration times of each photodetection event of D_1 and D_2. The time axes of the event timers can be divided into a sequence of time windows Δt, each labeled by time t_i, for $i = 1, 2, ..., N$. The software first calculates the mean photon number for each detector, $\bar{n}_1$ and $\bar{n}_2$, and then calculates the photon number fluctuations for each ith time window, $\Delta n_1(t_i) = n_1(t_i) - \bar{n}_1$ and $\Delta n_2(t_i) = n_2(t_i) - \bar{n}_2$, which can either be positive or negative. It then calculates the photon number fluctuation correlation

$$\langle \Delta n(x_1) \Delta n(x_2) \rangle = \frac{1}{N} \sum_{i=1}^{N} \Delta n_1(t_i) \Delta n_2(t_i), \quad (12)$$

where N is the total number of time windows for a data point of a chosen x_1 and x_2.

Even though the atmosphere always contains a certain amount of optical turbulence, we had the light propagate over the heating elements of a toaster oven to achieve an extreme effect (Fig. 1). These heating elements produce enough heat to rapidly vary the air density above them, thereby causing variations in the index of refraction. The resulting optical path variations "blur out" the classic interference pattern observed in the measurement of $\langle n(x_j) \rangle$ when $l_c > d$, where $j = 1, 2$ labels the

measurements by D_1 and D_2. However, this turbulence does not change the interference pattern observed in the measurement of $\langle \Delta n(x_1) \Delta n(x_2) \rangle$ when scanning in the neighborhood of $x_1 \approx x_2$.

Figure 2 reports a set of typical experimental results observed from the photon number fluctuation correlation (11). Figure 2(a) is a measurement of $\langle \Delta n(x_1) \Delta n(x_2) \rangle$ when the heating elements were powered off, i.e., no turbulence present, and Fig. 2(b) is a measurement of $\langle \Delta n(x_1) \Delta n(x_2) \rangle$ when the heating elements were powered on, i.e., strong turbulence present. When D_1 and D_2 were scanned in the neighborhood of $x_1 \approx x_2$, the visibility of the interference pattern with turbulence present was $94.3\% \pm 0.2\%$, which is consistent with the visibility without turbulence present, $94.6\% \pm 0.2\%$. The data in Figs. 2(a) and 2(b) have been normalized by the same factor, maintaining the ratio between the two. Comparing the two maximums we see that the amplitude of the pattern with turbulence present is approximately 86% of the amplitude of the pattern without turbulence present, which is due to the scattering effect of the turbulence. However, as represented in Fig. 2(b), this scattering does not devalue the visibility of the interference observed from the measurement of $\langle \Delta n(x_1) \Delta n(x_2) \rangle$. In other words, we have demonstrated a turbulence-free Young's double-slit interferometer.
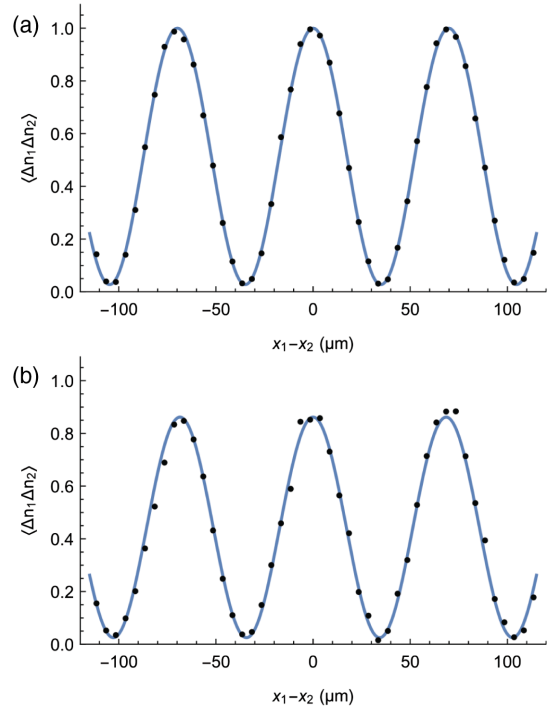

FIG. 2. Typical measurement of turbulence-free interference. (a) Without turbulence, the measurement of the photon number fluctuation correlation produces an interference pattern when $l_c \ll d$. (b) When turbulence was introduced, the interference pattern remained with almost 100% visibility.
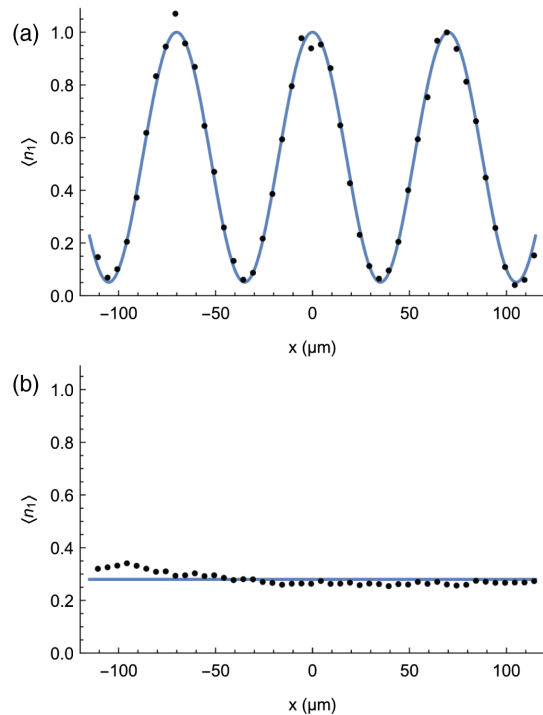
FIG. 3. Typical measurement to confirm strong enough turbulence is present. (a) Without turbulence, the classic Young's double-slit interferometer produces an interference pattern when $l_c > d$. (b) When turbulence is present, it blurs the interference pattern completely.

To demonstrate that the turbulence was strong enough to blur the classic interference present, we removed the rotating ground glass and directed the unaltered laser beam in the TEM$_{00}$ mode directly onto the double slit. The spatial coherence length of a TEM$_{00}$ mode laser beam is as large as the transverse size of the beam itself, equivalent to having a thermal source of $\Delta\theta_s \to 0$ or $l_c \to \infty$, satisfying the condition of $l_c > d$. Figure 3(a) reports a typical measured result of $\langle n(x_j) \rangle$ when the heating elements were powered off, i.e., without turbulence, Eq. (8). Figure 3(b) reports the same measurement of $\langle n(x_j) \rangle$ but now with the heating elements powered on. It is clear that the interference pattern is completely blurred out by the turbulence. This result guarantees the turbulence introduced by our heating elements is strong enough to demonstrate the turbulence-free nature of our new type of interferometer.

In principle, this mechanism of achieving turbulence-free two-photon interference could be applied to other types of interferometers, making them turbulence free as well. To avoid atmospheric turbulence and vibrations, many interferometers are contained within complicated, high cost vacuum systems. With a turbulence-free interferometer, these complicated and expensive systems would no longer be required. For instance, we shall be able to design and build sensitive interferometers in the open air for gravitational wave detection.

[1] T. Young, *A Course of Lectures on Natural Philosophy and the Mechanical Arts* (Printed for J. Johnson by W. Savage, London, 1807).
[2] E. Hecht, *Optics* (Addison Wesley, Reading, MA, 2002).
[3] A. R. Thompson, J. M. Moran, and G. W. Swenson, Jr., *Interferometry and Synthesis in Radio Astronomy* (John Wiley & Sons, New York, 2001).
[4] P. R. Saulson, *Fundamentals of Interferometric Gravitational Wave Detectors* (World Scientific, Singapore, 1994).
[5] D. C. Williams, *Optical Methods in Engineering Metrology* (Chapman and Hall, London, 1993).
[6] D. D. Nolte, *Optical Interferometry for Biology and Medicine* (Springer, New York, 2011).
[7] M. E. Brezinski, *Optical Coherence Tomography: Principles and Applications* (Academic Press, New York, 2006).
[8] V. I. Tatarski, *Wave Propagation in a Turbulent Medium* (Mcgraw-Hill, New York, 1961).
[9] F. Roddier, Prog. Opt. **19**, 281 (1981).
[10] B. P. Abbott *et al.*, Rep. Prog. Phys. **72**, 076901 (2009).
[11] B. P. Abbott *et al.*, Phys. Rev. Lett. **116**, 061102 (2016).
[12] Y. H. Shih, *An Introduction to Quantum Optics: Photon and Biphoton Physics*, 1st ed. (CRC Press, Taylor & Francis, London, 2011), pp. 45–50, 242–258.
[13] A. Einstein, Ann. Phys. (Berlin) **322**, 891 (1905).
[14] R. J. Glauber, Phys. Rev. **130**, 2529 (1963).
[15] M. O. Scully and M. S. Zubairy, *Quantum Optics* (Cambridge University Press, Cambridge, England, 1997).
[16] P. Dirac, *The Principle of Quantum Mechanics*, (Oxford University Press, New York, 1930).
[17] P. H. S. Ribeiro, S. Pádua, J. C. Machado da Silva, and G. A. Barbosa, Phys. Rev. A **49**, 4176 (1994).
[18] D. V. Strekalov, A. V. Sergienko, D. N. Klyshko, and Y. H. Shih, Phys. Rev. Lett. **74**, 3600 (1995).
[19] J. Řeháček and J. Peřina, Opt. Commun. **125**, 82 (1996).
[20] C. K. Hong and T. G. Noh, J. Opt. Soc. Am. B **15**, 1192 (1998).
[21] E. J. S. Fonseca, C. H. Monken, and S. Pádua, Phys. Rev. Lett. **82**, 2868 (1999).
[22] G. Brida, E. Cagliero, G. Falzetta, M. Genovese, M. Gramegna, and E. Predazzi, Phys. Rev. A **68**, 033803 (2003).
[23] G. Scarcelli, A. Valencia, and Y. H. Shih, Europhys. Lett. **68**, 618 (2004).
[24] W. Martienssen and E. Spiller, Am. J. Phys. **32**, 919 (1964).
[25] H. Chen, T. Peng, and Y. H. Shih, Phys. Rev. A **88**, 023808 (2013).
[26] T. Peng, H. Chen, Y. H. Shih, and M. O. Scully, Phys. Rev. Lett. **112**, 180401 (2014).